LASER & PHOTONICS REVIEWS

www.lpr-journal.org

Integrating 2D Materials and Plasmonics on Lithium Niobate Platforms for Pulsed Laser Operation at the Nanoscale

Mariola O. Ramírez, Pablo Molina, David Hernández-Pinilla, Guillermo López-Polín, Pablo Ares, Lidia Lozano-Martín, Han Yan, Yan Wang, Soumya Sarkar, Jinan H. Al Shuhaib, Fabrice Leardini, Julio Gómez-Herrero, Manish Chhowalla, and Luisa E. Bausá*

The current need for coherent light sources for integrated (nano)photonics motivates the search for novel laser designs emitting at technologically relevant wavelengths with high-frequency stability and low power consumption. Here, a new monolithic architecture that integrates monolayer MoS_2 and chains of silver nanoparticles on a rare-earth (Nd^{3+}) doped $LiNbO_3$ platform is developed to demonstrate Q-switched lasing operation at the nanoscale. The localized surface plasmons provided by the nanoparticle chains spatially confine the gain generated by Nd^{3+} ions at subwavelength scales, and large-area monolayer MoS_2 acts as saturable absorber. As a result, an ultra-compact coherent pulsed light source delivering stable train pulses with repetition rates of hundreds of kHz and pulse duration of 1 µs is demonstrated without the need of any voltage-driven optical modulation. Moreover, the monolithic integration of the different elements is achieved without sophisticated processing, and it is compatible with $LiNbO_3$-based photonics. The results highlight the robustness of the approach, which can be extended to other 2D materials and solid-state gain media. Potential applications in communications, quantum computing, or ultra-sensitive sensing can benefit from the synergy of the materials involved in this approach, which provides a wealth of opportunities for light control at reduced scales.

1. Introduction

Integrated photonics is currently the subject of an intense activity due to the technological requirements in crucial fields such as optical communications, sensing technologies, quantum technologies, or artificial intelligence.[1–7] Among the available photonic platforms, $LiNbO_3$ (LN) is undergoing a technological revolution motivated by recent breakthroughs in fabrication techniques which enable the availability of high-quality CMOS-compatible LN-on-insulator thin films.[8–11] Due to its ultra-low-loss modulation and propagation capabilities, and its excellent nonlinear properties, LN has proven to be an outstanding and highly versatile platform to develop a wide variety of integrated photonic components including high-performance modulators,[12,13] ultra-efficient wavelength converters,[14,15] on-chip electro-optics devices,[16] broadband frequency combs,[17] or photon-pair sources,[18,19]

M. O. Ramírez, P. Molina, D. Hernández-Pinilla, G. López-Polín, L. Lozano-Martín, J. H. Al Shuhaib, F. Leardini, L. E. Bausá
Dept. Física de Materiales
Universidad Autónoma de Madrid
Madrid 28049, Spain
E-mail: mariola.ramirez@uam.es

The ORCID identification number(s) for the author(s) of this article can be found under https://doi.org/10.1002/lpor.202300817

DOI: 10.1002/lpor.202300817

M. O. Ramírez, P. Molina, D. Hernández-Pinilla, P. Ares, F. Leardini, J. Gómez-Herrero, L. E. Bausá
Instituto Nicolás Cabrera
Universidad Autónoma de Madrid
Madrid 28049, Spain

M. O. Ramírez, P. Ares, J. Gómez-Herrero, L. E. Bausá
Condensed Matter Physics Center (IFIMAC)
Universidad Autónoma de Madrid
Madrid 28049, Spain

P. Ares, J. Gómez-Herrero
Dept. Física de la Materia Condensada
Universidad Autónoma de Madrid
Madrid 28049, Spain

H. Yan, Y. Wang, S. Sarkar, M. Chhowalla
Dept. of Materials Science & Metallurgy
University of Cambridge
Cambridge CB3 0FS, UK

among others. However, despite these advances, the integration of optically active components on photonic integrated circuits (PICs) is still a challenge.[20,21] In particular, monolithically integrated coherent light sources with key operating conditions such as lasing at technologically relevant wavelengths, high frequency stability, and low energy consumption are required.

In this context, the association of rare earth doped LN-based solid-state gain media with metallic nanostructures has provided an efficient and ultra-compact approach to develop multifunctional solid-state nanolasers (nano-SSL) capable of generating laser emission at the nanoscale.[22] These nano-SSLs rely on the strong subwavelength confinement of the laser modal volume enabled by localized surface plasmon resonances (LSPRs) of the metallic nanostructures deposited on the surface of the LN based gain medium. With this demonstration, the intrinsic advantages of SSLs, such as a high thermal, physical, and chemical stability, which greatly exceed those offered by other types of gain media, are available at the nanoscale. Additionally, nano-SSLs have shown a significant reduction of the pump power at threshold (twofold), and an extraordinary improvement of the laser slope efficiency (15-fold) compared to their conventional bulk counterpart systems,[23] entailing a substantial reduction in energy consumption for the operation of the devices. Moreover, the association of plasmonic nanostructures with LN based nano-SSLs allows the emergence of novel functionalities at subwavelength spatial regions due to the LN nonlinearity. Such is the case of the simultaneous multiline operation at the visible and near infrared regions.[24]

Although a few works have demonstrated the feasibility of sub-wavelength confined pulsed lasing from semiconductor nanolasers,[25,26] so far, nano-SSLs have been shown to operate only in continuous regime, their operation in pulsed conditions being highly desirable for applications. From this perspective, the development of pulsed nano-SSLs will enable room temperature coherent light sources with strong spatial and temporal confinement of the emitted radiation opening new avenues for novel robust and efficient light sources operating at the nanoscale. Pulsed nano-SSLs could be useful in photolithography for materials processing enabling ultrasmall motif sizes, in ultrahigh sensitivity biodetectors or for ultra-compact optical circuits, among others, with the added value of reduced energy consumption. Additionally, the generation of pulsed laser radiation from nano-SSLs would open the way to extreme light-matter interaction from which a dramatic intensification of nonlinear processes (NL) in nanometric regions is expected. A relatively extended method for generating pulsed laser operation in conventional solid-state lasers relies on the use of saturable absorbers (SAs). In recent years, 2D materials have been incorporated into conventional solid-state laser cavities to successfully demonstrate its ability to produce short laser pulses through passive Q-switch or mode-locking processes over a wide range of wavelengths.[27] Specifically, it has been shown that certain transition metal dichalcogenides (TMD) (MX_2 M = Mo, W; X = S, Se) can be used as broadband SAs due to their high optical nonlinearity.[28,29] This characteristic, combined with their high strength and flexibility, makes MoS_2 and other TMDs ideal candidates for obtaining compact pulsed nano-SSLs in pulsed regime. In this regard, trivalent rare earth-doped solid-state gain media are well suited for Q-switch operation since they offer the capability of storing the excitation energy over sufficiently long times due to the long lifetime values of their upper metastable laser states.

In this work, we present a new monolithic architecture that fully integrates large-area monolayer molybdenum disulfide (1L-MoS_2) and linear chains of closely spaced silver nanoparticles (Ag NPs) on a rare earth doped LN platform (Nd^{3+}:LN) to demonstrate the first 2D Q-switched SSL operating at the nanoscale (2D-QNano-SSL). The ultra-compact coherent pulsed light source is achieved without the need for any voltage-driven optical modulation, it is compatible with LN-based integrated photonics and does not require sophisticated processing methods.

The motivation for the specific choice of these elements for the 2D-QNano-SSL is detailed as follows: 1L-MoS_2 is a direct band gap 2D TMD with a great potential for the next generation of optoelectronic devices, which has demonstrated saturable absorption in a broad spectral range;[29] Ag NPs chains support a robust collective longitudinal plasmonic mode with low dissipative losses, which provides the sub-wavelength confinement of the laser emission;[23] and Nd^{3+} is a canonical optically active ion, extensively used in SSLs with large quantum efficiency at technologically relevant spectral regions and a wide variety of bands for optical pumping.[30] Thus, the opportunity of bringing together different technologically relevant systems by combining TMDs, plasmonic nanostructures and LN-based gain media, emerges as a stimulating and attractive approach for tailoring novel functionalities, and secures the potential integration of high-performance multifunctional nano-SSLs on the next generation of LN-based PICs. Our hybrid system was achieved through simple, scalable, and cost-effective fabrication methods based on both ferroelectric lithography[31] and deterministic transfer by all-dry viscoelastic stamping.[32] By combining the unique properties of these materials in one single platform, we demonstrate spatially confined sub-diffractive stable pulse trains with repetition rate of hundreds of kHz and pulse duration close to 1 μs. The device operates at room temperature in an alignment-free Fabry-Pérot optical resonator and exhibits a single-mode operation enabling narrow laser linewidth in the near-infrared spectral region. The results presented here provide a proof-of-concept for a self-Q-switching plasmonic nanolasing using 2D materials, and open new routes for novel engineerable nanophotonic devices with strong spatial localization of coherent radiation.

2. Results and Discussion

The monolithic architecture employed in this work is sketched in **Figure 1**. The core is a Z-cut Nd^{3+} doped LN platform, which presents an antiparallel ferroelectric domains structure we use it here as template for the formation of Ag plasmonic nanostructures by ferroelectric lithography.[31] In particular, the presence of a non-uniform electric field on the surface of the ferroelectric domains structure, which shows a strong z component at the domain boundary surface, enables the formation of chains of 50 nm diameter Ag NPs by a simple photo-reduction process on the surface of the Nd^{3+}:LN.[33] A Scanning Electron Microscopy (SEM) image of a Ag NP chain formed onto a domain wall surface is shown in **Figure 2**a (left panel). As reported, the chains are formed by closely spaced quasi-spherical Ag NPs of 50 nm average size and particle spacing ≈2 nm.[33] These metallic chains support an intense and spectrally broad

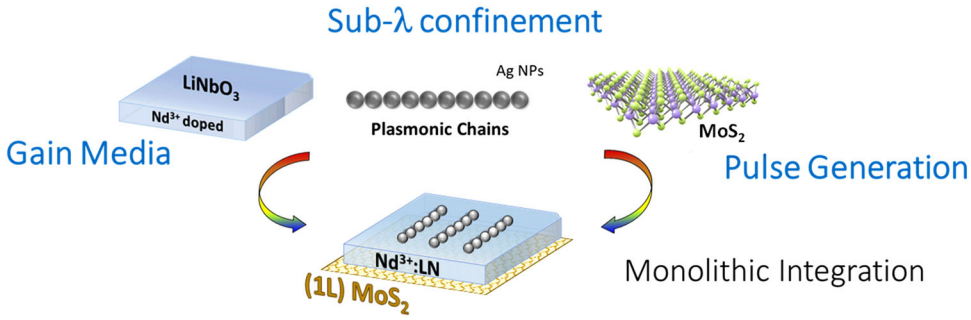

Figure 1. Schematic representation of the monolithic integration utilized to obtain self-Q-switched operation at the nanoscale. The final device integrates large-area monolayer molybdenum disulfide (1L-MoS_2) and linear chains of closely spaced silver nanoparticles (Ag NPs) on a Nd^{3+} doped LN gain medium.

longitudinal mode (electric field oscillating parallel to the chain, see Figure 2b). This mode extends from the visible to the near-infrared region (blue shaded) overlapping a good part of the spectral region in which the relevant Nd^{3+} optical transitions occur. In particular, the Nd^{3+} $^4I_{9/2} \rightarrow {}^4F_{5/2} + {}^2H_{9/2}$ absorption transition centered at 800 nm (green shaded) used for optical pumping, and the spontaneous emission spectrum corresponding to the $^4F_{3/2} \rightarrow {}^4I_{11/2}$ transition (red shaded) are illustrated. The near field response at the laser wavelength for a plane wave polarized parallel to the chain is shown in Figure 2a right panel, which accounts for the effect of the plasmonic local fields on the Nd^{3+} emission (namely, threshold reduction and field confinement).[24]

The laser architecture was completed by attaching a 1L-MoS_2 as SA to induce the generation of short optical pulses by passive Q-switching of the plasmon-assisted Nd^{3+}:LN nanolaser (see Figure 1). To ensure sizeable coverage regions, high-quality large-area 1L-MoS_2 (≈50×50 μm^2) was obtained by chemical vapor deposition (CVD) on a SiO_2 substrate and then deterministically transferred onto the crystal surface of Nd^{3+}:LN opposite to that of the Ag NP chains. The possibility to prepare high-quality large-scale monolayers of MoS_2 allow us to homogeneously integrate the nonlinear saturable absorber with the optical gain media in a controlled manner, thus enabling spatially resolved scanning confocal laser gain microscopy experiments with high spatial reproducibility. Details on the growth and transfer procedure can be found in Experimental Section. The nonlinear SA features of the transferred monolayer were measured by gradually increasing the incident power (at a wavelength of 1064 nm) and recording the nonlinear transmittance of 1L-MoS_2 under different intensity values (input fluences). The transmittance curve is displayed in Figure 2c. As observed, at low incident intensities the transmittance of the system is ≈70.5 %, consistent with the combination of the transmittances of the LN crystal (74 %) and 1L-MoS_2 (95 %),[34] respectively. As we increase the input fluence above 10 kW cm^{-2}, the transmittance increases up to ~0.74 and then remains constant indicating that the 1L-MoS_2 has been completely bleached. From this result, the modulation depth at the laser wavelength can be estimated to be ≈3.5 %, in

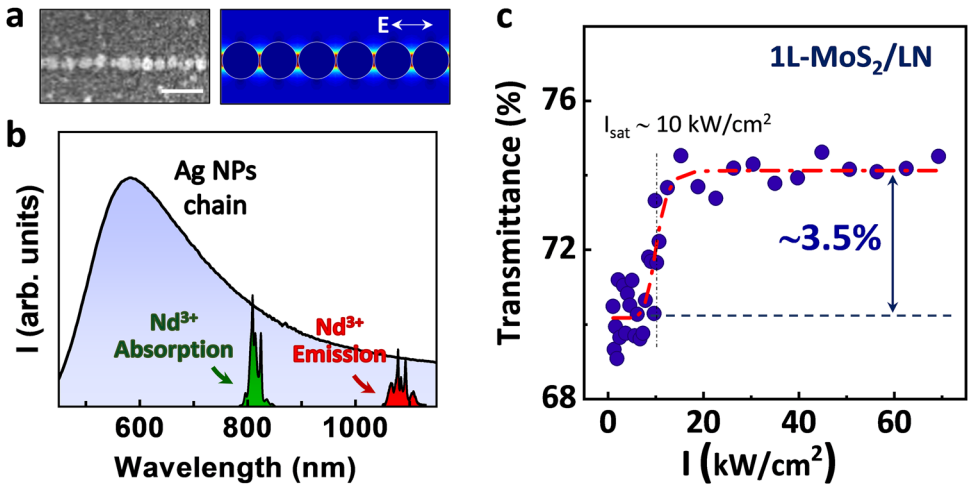

Figure 2. Optical features of the individual components involved in the device. a) SEM image (left) and near field distribution of a plasmonic chain formed by Ag NPs of 50-nm diameter and spacing ≈2 nm simulated at a wavelength ≈1 μm for electric field oscillation parallel to the chain (right). Scale bar corresponds to 200 nm. b) Extinction spectrum of the longitudinal mode of the Ag NP chain (shaded in blue color). Nd^{3+} $^4I_{9/2} \rightarrow {}^4F_{5/2} + {}^2H_{9/2}$ absorption transition (green) and $^4F_{3/2} \rightarrow {}^4I_{11/2}$ emission (red) bands are included to highlight the spectral overlap of the Ag NPs LSPR and the relevant transitions of Nd^{3+} ions. c) Transmittance of the 1L-MoS_2 deposited on LN at 1064 nm as a function of the input fluence. A modulation depth of 3.5 % and a saturable intensity of ≈10 kW cm^{-2} are obtained.

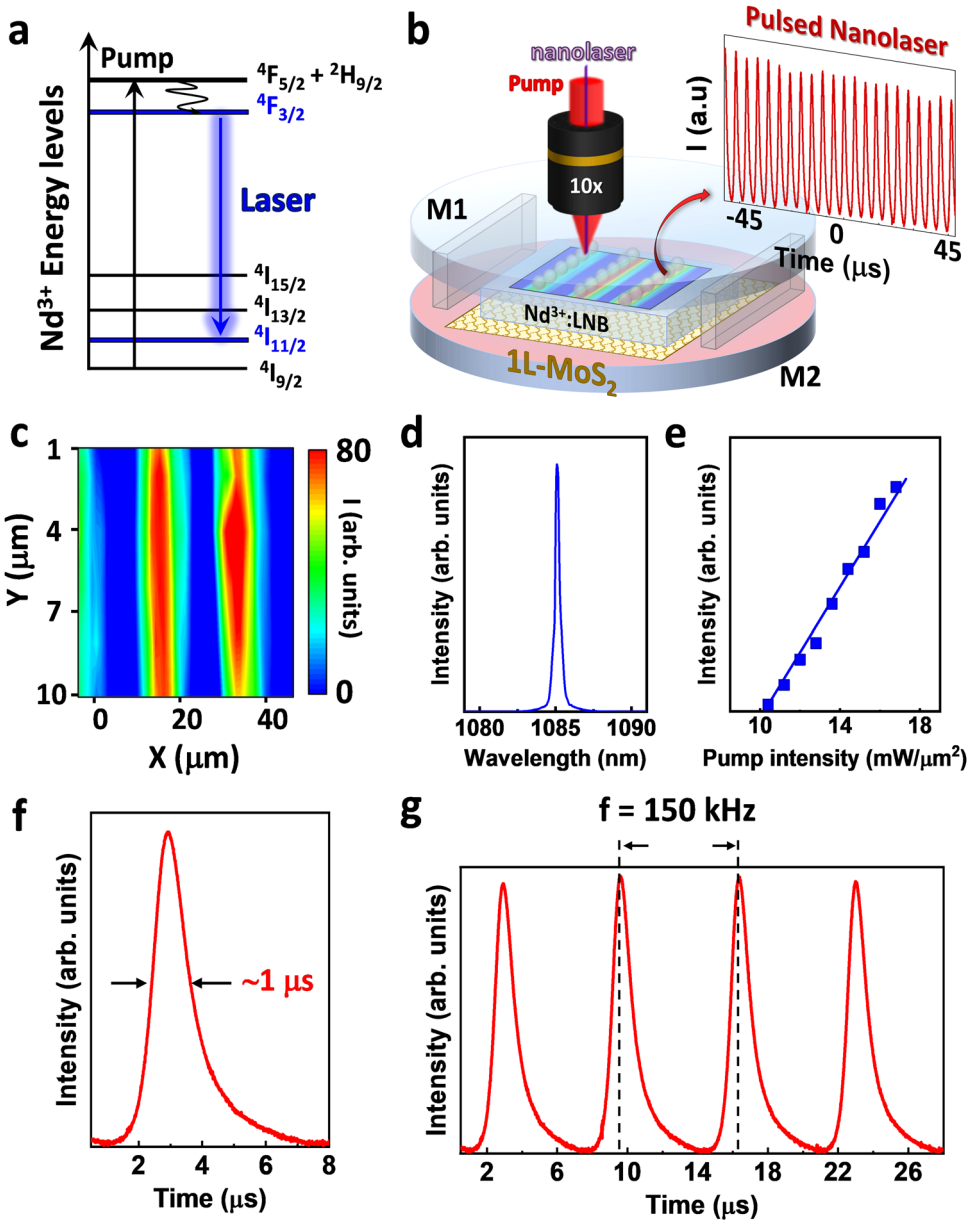

Figure 3. Q-switched lasing performance at the nanoscale. a) Energy levels scheme of Nd^{3+} ions showing the relevant pump and emission transitions involved in the laser experiments. b) Schematic representation of spatially resolved scanning confocal laser gain microscopy in the hybrid integrated system using a Fabry–Pérot resonator formed by two plane-parallel mirrors (M1 and M2). The inset shows a train of pulses generated by Q-switching at the nanoscale. c) Spatial distribution of the integrated laser emission. The intensity follows the spatial distribution of the Ag NP chains. d) Laser emission spectrum according to the $^4F_{3/2}$ (R_1) → $^4I_{11/2}$ (Y_2) Stark transition of Nd^{3+} in LN. e) Input–output intensity curve of the Q-switched laser operation at the nanoscale. Solid line is a linear fit. f) Example of a 1L-MoS_2 induced Q-switched pulse profile at an incident intensity of 13.5 mW μm^{-2}. g) Detail of a train of pulses for the same incident intensity displaying a repetition rate of 150 KHz.

agreement with previous results.[35] The measured saturation intensity value is also similar to some reported values at the same laser wavelength.[36] Although the microscopic mechanism responsible for the absorption of MoS_2 in the near-infrared region is not definitively clear yet and goes beyond the scope of this article, several works have proposed the presence of defect levels as responsible for the absorption at energies smaller than the band gap.[37] Both modulation depth and saturation intensity will directly impact the laser power threshold and temporal features of fabricated pulsed nano-SSLs based on this monolithic architecture.

Laser experiments were carried out by spatially resolved scanning confocal laser gain microscopy. Continuous wave optical pumping at λ_p = 808 nm, corresponding to the Nd^{3+} $^4I_{9/2}$ → $^4F_{5/2} + {}^2H_{9/2}$ transition (see **Figure 3**a) was focused onto the top surface of the laser crystal by means of a 10x microscope objective. The laser emission was collected in backscattering geometry with the same objective lens. Throughout the experiments, the

pump radiation was polarized parallel to the Ag NP chain ensuring maximum spectral overlap of the relevant Nd^{3+} transitions with the longitudinal plasmonic mode of the chain. A schematic representation of the experimental configuration is depicted in Figure 3b. Figure 3c shows the spatial distribution of the integrated laser intensity obtained around two Ag NP chains. As observed, lasing operation is only achieved in the vicinity of the Ag NP chains, corroborating the sub-wavelength confinement of the lasing radiation and the strong reduction of the pump power at threshold with respect to bare Nd^{3+}:LN regions. As shown in Figure 3d, the nanolaser oscillates at a wavelength of 1085 nm according to the Nd^{3+} $^4F_{3/2} \rightarrow {}^4I_{11/2}$ optical transition (Figure 3a), specifically at the $R_1 \rightarrow Y_2$ Stark transition.[24] It exhibits single-mode operation with a measured linewidth of ≈0,5 cm^{-1}, which corresponds to the limit of our experimental setup. Solid-state lasers operating at a single frequency showcase remarkably low-intensity noise. Moreover, in these systems, the lack of mode distribution within the resonator effectively eliminates mode beating effects. Consequently, under Q-switching operation, the generation of clean pulse shapes with minimal noise can be expected.

The input-output laser curve obtained from the hybrid integrated system shows a linear dependence of the laser output with the pump intensity as well as an abrupt threshold behavior, typical of SSLs, at $P_{th} = 10$ mW μm^{-2} (Figure 3e). Immediately above this threshold value, the monolithic device generates stable long train pulses obtained through repetitive self-Q switching. Indeed, since no bulk laser operation is observed in the off-chain regions within the pumping range employed in this study, the laser pulse trains are exclusively obtained at the nanoscale, specifically, in the vicinity of the Ag NP chains. Figure 3f shows, as an example, the temporal profile of a single pulse obtained at the proximity of a plasmonic chain for an incident pump intensity of 13.5 mW μm^{-2}. It shows a clean shape with a pulse duration of ≈1 μs. The repetition rate at this pump intensity shows values as high as 150 kHz with a peak-to-peak intensity variation below 10% (see Figure 3g).

The pulsed nanolasing operation is based on the modulation of the optical losses in the gain medium, enabled by the presence of 1L-MoS_2, which enhances the transmittance of the system at the laser wavelength at high optical intensities. Accordingly, as shown in **Figure 4**, the pulsed behavior of the hybrid nanolaser is strongly dependent on the pump intensity, specifically, near the threshold value. In particular, the pulse width duration decreases from 6 to 1 μs by simply increasing the pump intensity from 10 to 12 mW μm^{-2}. Above this value, the pulse width duration remains constant denoting the complete bleaching of the 1L-MoS_2 due to the energy density delivered by the nanolaser (Figure 4b). Regarding the pulse duration, the values obtained here are of the order of those reported for Nd^{3+} based bulk lasers using MoS_2,[29] but longer than for other conventional bulk Q-switched lasers, typically in the nanosecond range. This fact can be attributed to the relatively low modulation depth (~3.5%) exhibited by the 1L MoS_2 SA at the laser wavelength ≈1.08 μm. Nevertheless, this issue can be addressed by extending our approach to other solid-state gain media within the plethora of rare earth host combinations that offer laser emission in a wide range of the visible and near-infrared spectral regions. The possibility of using alternative 2D materials and configurations with a larger modulation depth is also considered.

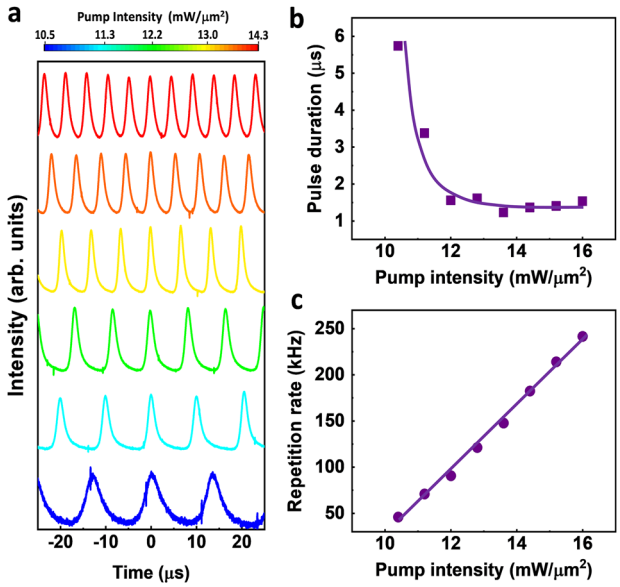

Figure 4. Evolution of the pulse duration and repetition rate modulation with the pump intensity. a) Temporal evolution of the pulse trains with the incident pump intensity. The temporal profiles have been normalized and centered at $t = 0$ for a better comparison. b) Pulse duration and c) Pulse repetition rate as a function of the incident pump intensity. Purple lines are guides to the eye to evidence the asymptotic and linear behavior, respectively.

Finally, Figure 4c shows the evolution of the repetition rate with the pump intensity. As observed, slight variations of the pump intensity produce significant changes in the repetition rate, which linearly increases from 50 to 250 kHz in the 10–15 mW μm^{-2} range. It is important to mention that the increase of the pulse repetition rate with the input power can be achieved without altering the pulse duration, which is of interest for a fine control of the pulsed light. This feature outperforms conventional 2D Q-switched SSLs, as they exhibit a much slower decrease of the pulse duration with increasing the pump intensity and rarely reach a complete saturation.[37,38] This highlights the crucial importance of subwavelength laser confinement compared to the conventional volumetric configurations.

3. Conclusion

We have successfully demonstrated self Q-switched operation at the nanoscale by the monolithic integration of plasmonic chains of closely spaced Ag nanoparticles and large-area monolayer molybdenum disulfide on a Nd^{3+} doped Lithium Niobate platform. Merging the unique features of those components in one single element enables to concentrate the optical gain delivered by the nanolaser in the time domain without the need for any voltage-driven optical modulation. The integrated architecture meets the current requirements of sustainability and robustness and greatly exceeds the performance of conventional bulk configurations in terms of threshold reduction, improved laser efficiency, and reduced laser linewidth. It also offers the possibility of modulating the repetition rate from tens to hundreds of kHz without altering the pulse duration, which can be useful for data storage, on-chip optical communications,

near-field spectroscopy and sensing or optical interconnects. On top of that, the use of Lithium Niobate as a photonic solid-state platform provides an added value toward reliable integrated nanophotonic components. Beyond solid-state lasers, the integration of 2D materials with other plasmon-assisted nanolasers featuring different designs and configurations could offer new strategies to manipulate and control extreme light-matter interactions at nanoscopic dimensions, which may unveil unexplored physical phenomena and expand the functionalities of coherent optical sources at the nanoscale.

4. Experimental Section

Sample Preparation A Nd^{3+}-doped periodically poled $LiNbO_3$ crystal (Nd^{3+}:PPLN) was grown by the off-centered Czochralski technique by adding Nd^{3+} as Nd_2O_3 in the melt.[39] The rotation (30 rpm) and pulling rates (1 mm h^{-1}) employed produced a closely-50 % duty cycle of alternating antiparallel ferroelectric domains with variable periodicities in the range of 5–100 µm. Z-cut plate sample (7 × 5 × 0.8) mm (length × width × thickness) was cut and polished up to optical quality.

The plasmonic chains of Ag NPs were formed on the domain walls surfaces of the Nd^{3+}:PPLN crystal following a ferroelectric lithography process. The Z-cut crystal plate was immersed in a 0.01 M $AgNO_3$ solution at 65 °C and illuminated for 7 min with an UV Mercury pen-lamp (UVP model 11SC-1) at 253.6 nm with an emission intensity of 5400 µW cm^{-2}. Details on the procedure can be found elsewhere.[33]

CVD-grown MoS_2 monolayer was transferred onto the PPLN substrate following a multistep process. First, the MoS_2 material was synthesized on SiO_2/Si via CVD utilizing elemental sulfur and MoO_3 powder as precursors. During the growth, MoO_3 (2.5 mg) and SiO_2/Si were set at 720 °C. Sulfur (60 mg) at upper stream is ≈250 °C. 60 sccm N_2 was used as carrier gas. NaOH solution was used as promoter, which is spin-coated on SiO_2/Si. The process, described in Ref.[40] results in a few-layer MoS_2 film. In this process, the SiO_2/Si substrate covers the MoO_3 boat where the growth substrate overhung the MoO_3 boat on the side. As a result, single-layer film and isolated single-layer flake islands were obtained. In a second step, a piece of PDMS stamp (Gel-Film by Gel-Pak) was placed onto the surface of MoS_2/SiO_2 and gently pressed to ensure adequate adhesion between the PDMS stamp and MoS_2 flake. Subsequently, water drops were placed around the PDMS. In this way the water was intercalated between the MoS_2 and the SiO_2, and finally, the PDMS was released from the substrate with the MoS_2 attached to its surface. After PDMS/MoS_2 stamp was detached from the substrate, it was rinsed in deionized water for several times and baked on a hot plate at 70 °C for 2 h to remove moisture. Finally, a large-area (≈50×50 μm^2) MoS_2 stamp was attached to the Nd^{3+}:PPLN substrate by a deterministic PDMS-based viscoelastic stamping method.[32]

Optical Characterization The nonlinear SA features of the monolayer deposited on LN were measured by increasing the incident power of a nanosecond pulsed laser (Spectra Physics Navigator 1064–7) tuned at wavelength of 1064 nm. The samples were scanned along their surfaces in order to assess the homogeneity of the surface of the 2D SA.

For the laser experiments, a Z-cut (7 × 5 × 0.8) mm (length × width × thickness) Nd^{3+}:PPLN plate was placed between two plane-parallel mirrors conforming the optical cavity. The mirrors were highly reflective (R > 99.7 %) at laser wavelength (λ = 1085 nm) and showed high transmittances (T > 95 %) at the pump wavelength (λ_{pump} = 808 nm). Two 1 mm-thick spacers were placed between the mirrors to avoid the contact of the metallic nanostructures with the mirror surface.

The cavity was placed on a two-axis XY motorized platform with 0.2 µm spatial resolution. A tunable continuous-wave Ti:Sapphire laser (Spectra Physics) was used as excitation source. The pump beam was focused onto the surface of the laser crystal by an objective lens, Olympus MPLAN 10× NA 0.25, which provided a long working distance. Laser radiation was collected in backscattering geometry with the same objective lens and directed by an optical fiber to a Peltier-cooled Horiba Synapse CCD connected to a Horiba iHR 550 monochromator (950 groves/mm, blazed at 900 nm). The pulses trains were recorded by a fast InGaAs photodetector (Thorlabs DET08C) coupled to a MDO oscilloscope (Lecroy Teledyne WavePro 404HD).

Acknowledgements

M.O.R., P.M., D.H.P., G.L.P., and L.E.B. acknowledge funding from the Spanish State Research Agency under grant PID2019-108257GB-I00 and PID2022-137444NB-I00. P.A. acknowledges financial support from Comunidad de Madrid and Universidad Autónoma de Madrid (SI3-PJI-2021-00479) and from the Spanish State Research Agency under grants TED2021-132219A-I00, Ramón y Cajal fellowship RYC2020-030302-I, and "María de Maeztu" Programme for Units of Excellence in R&D (CEX2018-000805-M). J.G.H. acknowledges financial support from the Spanish State Research Agency under grant PID2019-106268GB-C31. H.Y., Y.W., S.S., and M.C. acknowledge funding from European Research Council (ERC) Advanced Grant under the European Union's Horizon 2020 research and innovation program (grant agreement GA 101019828-2D- LOTTO]), EPSRC (EP/ T026200/1, EP/T001038/1). J.H.S. and F.L. acknowledge funding from the Spanish State Research Agency under grant PID2021-126098OB-I00.

Conflict of Interest

The authors declare no conflict of interest.

Data Availability Statement

The data that support the findings of this study are available from the corresponding author upon reasonable request.

Keywords

2D materials, Lithium Niobate, nanolasers, plasmonic chain, Q-switch, rare earth emitters, MoS_2

Received: August 25, 2023
Revised: October 9, 2023
Published online:

[1] W. Bogaerts, D. Pérez, J. Capmany, D. A. B. Miller, J. Poon, D. Englund, F. Morichetti, A. Melloni, *Nature* **2020**, *586*, 207.
[2] A. W. Elshaari, W. Pernice, K. Srinivasan, O. Benson, V. Zwiller, *Nat. Photonics* **2020**, *14*, 285.
[3] Z. Zhou, X. Ou, Y. Fang, E. Alkhazraji, R. Xu, Y. Wan, J. E. Bowers, *eLight* **2023**, *3*, 1.
[4] W.-Q. Wei, A. He, B. Yang, Z.-H. Wang, J.-Z. Huang, D. Han, M. Ming, X. Guo, Y. Su, J. Zhang, T. Wang, *Light Sci. Appl.* **2023**, *12*, 84.
[5] J. Milvich, D. Kohler, W. Freude, C. Koos, *Adv. Opt. Photonics* **2021**, *13*, 584.
[6] S. Paesani, Y. Ding, R. Santagati, L. Chakhmakhchyan, C. Vigliar, K. Rottwitt, L. K. Oxenløwe, J. Wang, M. G. Thompson, A. Laing, *Nat. Phys.* **2019**, *15*, 925.
[7] B. J. Shastri, A. N. Tait, T. Ferreira De Lima, W. H. P. Pernice, H. Bhaskaran, C. D. Wright, P. R. Prucnal, *Nat. Photonics* **2021**, *15*, 102.
[8] A. Boes, L. Chang, C. Langrock, M. Yu, M. Zhang, Q. Lin, M. Loncar, M. Fejer, J. Bowers, A. Mitchell, *Science* **2023**, *379*, eabj4396.
[9] Q. Luo, F. Bo, Y. Kong, G. Zhang, J. Xu, *Adv. Photon.* **2023**, *5*, 034002.

[10] D.i Zhu, L. Shao, M. Yu, R. Cheng, B. Desiatov, C. J. Xin, Y. Hu, J. Holzgrafe, S. Ghosh, A. Shams-Ansari, E. Puma, N. Sinclair, C. Reimer, M. Zhang, M. Loncar, *Adv. Opt. Photonics* **2021**, *13*, 242.
[11] D. Sun, Y. Zhang, D. Wang, W. Song, X. Liu, J. Pang, D. Geng, Y. Sang, H. Liu, *Light Sci. Appl.* **2020**, *9*, 197.
[12] H. Feng, K. Zhang, W. Sun, Y. Ren, Y. Zhang, W. Zhang, C. Wang, *Photon. Res.* **2022**, *10*, 2366.
[13] Z. Ruan, K. Chen, Z. Wang, X. Fan, R. Gan, L. Qi, Y. Xie, C. Guo, Z. Yang, N. Cui, L. Liu, *Laser Photonics Rev.* **2023**, *17*, 2200327.
[14] Y. Hu, M. Yu, D. Zhu, N. Sinclair, A. Shams-Ansari, L. Shao, J. Holzgrafe, E. Puma, M. Zhang, M. Loncar, *Nature* **2021**, *599*, 587.
[15] X. Wang, X. Jiao, B. Wang, Y. Liu, X.-P. Xie, M.-Y. Zheng, Q. Zhang, J.-W. Pan, *npj Quantum Inf.* **2023**, *9*, 38.
[16] M. Wang, Y. Xu, Z. Fang, Y. Liao, P. Wang, W. Chu, L. Qiao, J. Lin, W. Fang, Y. Cheng, *Opt. Express* **2017**, *25*, 124.
[17] Y. Hu, M. Yu, B. Buscaino, N. Sinclair, D. Zhu, R. Cheng, A. Shams-Ansari, L. Shao, M. Zhang, J. M. Kahn, M. Loncar, *Nat. Photonics* **2022**, *16*, 679.
[18] J.-Y. Chen, Y. Meng Sua, Z.-H. Ma, C. Tang, Z. Li, Y.-P. Huang, *OSA Continuum* **2019**, *2*, 2914.
[19] C. J. Xin, J. Mishra, C. Chen, D. Zhu, A. Shams-Ansari, C. Langrock, N. Sinclair, F. N. C. Wong, M. M. Fejer, M. Loncar, *Opt. Lett.* **2022**, *47*, 2830.
[20] J. Yang, M. Tang, S. Chen, H. Liu, *Light Sci. Appl.* **2023**, *12*, 16.
[21] V. Snigirev, A. Riedhauser, G. Lihachev, M. Churaev, J. Riemensberger, R. N. Wang, A. Siddharth, G. Huang, C. Möhl, Y. Popoff, U. Drechsler, D. Caimi, S. Hönl, J. Liu, P. Seidler, T. J. Kippenberg, *Nature* **2023**, *615*, 411.
[22] M. O Ramírez, P. Molina, A. Gómez-Tornero, D. Hernández-Pinilla, L. Sánchez-García, S. Carretero-Palacios, L. E. Bausá, *Adv. Mater.* **2019**, *31*, 1901428.
[23] P. Molina, E. Yraola, M. O. Ramírez, C. Tserkezis, J. L. Plaza, J. Aizpurua, J. Bravo-Abad, L. E. Bausá, *Nano Lett.* **2016**, *16*, 895.
[24] D. Hernández-Pinilla, P. Molina, C. De Las Heras, J. Bravo-Abad, L. E. Bausá, M. O. Ramírez, *ACS Photonics* **2018**, *5*, 406.
[25] T. P. H. Sidiropoulos, R. Röder, S. Geburt, O. Hess, S. A. Maier, C. Ronning, R. F. Oulton, *Nat. Phys.* **2014**, *10*, 870.
[26] J. S. Totero Gongora, A. E. Miroshnichenko, Y. S. Kivshar, A. Fratalocchi, *Nat. Commun.* **2017**, *8*, 15535.
[27] G. Sobon, *Two-Dimensional Materials - Synthesis, Characterization and Potential Applications*, (Ed: P. K. Nayak), InTechOpen, London, UK **2016**, Ch.7.
[28] Z. Luo, D. Wu, B. Xu, H. Xu, Z. Cai, J. Peng, J. Weng, S. Xu, C. Zhu, F. Wang, Z. Sun, H. Zhang, *Nanoscale* **2016**, *8*, 1066.
[29] S. Wang, H. Yu, H. Zhang, A. Wang, M. Zhao, Y. Chen, L. Mei, J. Wang, *Adv. Mater.* **2014**, *26*, 3538.
[30] A. A. Kaminskii, *Crystalline Lasers: Physical Processes and Operating Schemes*, CRC Press, Boca Raton, FL, USA **1996**.
[31] S. V. Kalinin, D. A. Bonnell, T. Alvarez, X. Lei, Z. Hu, R. Shao, J. H. Ferris, *Adv. Mater.* **2004**, *16*, 795.
[32] A. Castellanos-Gomez, M. Buscema, R. Molenaar, V. Singh, L. Janssen, H. S. J. Van Der Zant, G. A. Steele, *2D Mater.* **2014**, *1*, 011002.
[33] E. Yraola, P. Molina, J. L. Plaza, M. O. Ramírez, L. E. Bausá, *Adv. Mater.* **2013**, *25*, 910.
[34] S. Zhang, N. Dong, N. Mcevoy, M. O'brien, S. Winters, N. C. Berner, C. Yim, Y. Li, X. Zhang, Z. Chen, L. Zhang, G. S. Duesberg, J. Wang, *ACS Nano* **2015**, *9*, 7142.
[35] S. Das, Y. Wang, Y. Dai, S. Li, Z. Sun, *Light Sci. Appl.* **2021**, *10*, 27.
[36] H. Zhang, S. B. Lu, J. Zheng, J. Du, S. C. Wen, D. Y. Tang, K. P. Loh, *Opt. Express* **2014**, *22*, 7249.
[37] H. Pan, H. Chu, Z. Pan, S. Zhao, M. Yang, J. Chai, S. Wang, D. Chi, D. Li, *Nanophotonics* **2020**, *9*, 4703.
[38] J. M. Serres, P. Loiko, X. Mateos, H. Yu, H. Zhang, Y. Chen, V. Petrov, U. Griebner, K. Yumashev, M. Aguiló, F. Díaz, *Opt. Mater. Express* **2016**, *6*, 3262.
[39] V. Bermúdez, M. D. Serrano, E. Diéguez, *J. Cryst. Growth* **1999**, *200*, 185.
[40] J. Mann, D. Sun, Q. Ma, J.-R. Chen, E. Preciado, T. Ohta, B. Diaconescu, K. Yamaguchi, T. Tran, M. Wurch, K. Magnone, T. F. Heinz, G. L. Kellogg, R. Kawakami, L. Bartels, *Eur. Phys. J. B* **2013**, *86*, 226.